Turbulent wakes of fractal objects

Turbulent wakes of fractal objects

Adrian Staicu,[1] Biagio Mazzi,[2] J. C. Vassilicos,[3] and Willem van de Water[1]
[1]*Physics Department, Eindhoven University of Technology, Postbus 513, 5600 MB Eindhoven, The Netherlands*
[2]*DAMTP, University of Cambridge, Cambridge CB3 9EW, United Kingdom*
[3]*Department of Aeronautics, Imperial College, London SW7 2BY, United Kingdom*
(Received 13 March 2002; revised manuscript received 25 September 2002; published 18 June 2003)

Turbulence of a windtunnel flow is stirred using objects that have a fractal structure. The strong turbulent wakes resulting from three such objects which have different fractal dimensions are probed using multiprobe hot-wire anemometry in various configurations. Statistical turbulent quantities are studied within inertial and dissipative range scales in an attempt to relate changes in their self-similar behavior to the scaling of the fractal objects.

DOI: 10.1103/PhysRevE.67.066306 PACS number(s): 47.27.−i

I. INTRODUCTION

The self-similar structure of turbulence underlies Kolmogorov's well-known 1941 theory. In a modern geometrical phrasing of this theory, turbulent dissipation would be organized on a space-filling fractal set. In the same vein, small-scale intermittency results if this set is no longer space filling.

It is broadly believed that fully developed turbulence, when given enough time, creates its fractal structure *by itself*, no matter how the turbulent flow is excited. An intriguing idea is to impose a self-similar structure on the flow, for example, by creating turbulence in the wake of a fractal object. The question is whether the imprint of the excitation can be seen in the turbulent structure of the wake. In other words, whether the scaling properties of the object can determine, at least for some time, the scaling properties of the turbulent wake that is shed off the object. Thus, we may be able to directly influence the scaling exponents of fully developed turbulence and their related turbulence dissipation field. As a practical application, this idea may lead to improved turbulence generators and objects with novel drag properties. It should be noted that a direct influence of the fractal stirring on the scaling properties of the velocity field was demonstrated in the context of a reduced-mode model (the GOY model) [1].

Preliminary experiments by Queiros-Conde and Vassilicos [2] have hinted such an effect, but the structure functions used were rather unorthodox. The problem was that these quantities made it difficult to unravel the effect of the finite size of the fractal object from the effect of its scale invariant structure. In the present study, we attack this problem by measuring energy spectra and longitudinal as well as transverse structure functions. Our conclusion is that there may be a direct relation between the scaling properties of the fractal object and the turbulence that it creates. While the latter conclusion may not sound firm, we believe that it is interesting to expose the caveats and ambiguities of the experimental techniques used to reach it.

The fractal turbulence generators used are those of Ref. [2]. They have (necessarily) finite size and create very strong turbulence. We demonstrate that it is precisely these two circumstances that make it difficult to establish a direct relation between the scaling of the generator and the scaling of the turbulent wake it sheds.

II. EXPERIMENTAL SETUP

Our fractal objects are self-similar constructions with the smallest scales limited to 1 mm by manufacturing constraints (see Ref. [2] for a full description of these objects). With the size L of the fractal objects ranging between 17 and 37 cm, the number of iterations is limited to 4. A schematic view of these objects is provided in Fig. 1(a). The wake of three objects of increasing fractal dimension (2.05, 2.17, 2.40) placed in the 0.7 m$\times$0.9 m section of the tunnel was generated with a laminar flow that reaches 22 ms^{-1} in an empty windtunnel. The measurements were done with a rake of 10 hot-wire probes at different positions behind the fractal objects. Different orientations of the objects themselves with respect to the direction of the incoming flow of the windtunnel were used. The possible measurement configurations are sketched in Fig. 1(b).

The wakes of the fractals are strongly turbulent, a feature that challenges the application of hot-wire anemometry. Hot-wire sensors cannot discriminate between positive and negative fluid velocities, along the x direction [see Fig. 1(b)], u and $-u$. In particular, the sensor information is ambiguous as to the direction of the velocity in a plane perpendicular to the wire if the relative turbulent fluctuations, u/U and v/U, are large [where U is the time-averaged fluid velocity in the x direction and v is the fluid velocity in the y direction—see Fig. 1(b)]. Despite these disadvantages, hot-wire anemometry is still the only way to obtain statistically accurate measurements of the small-scale velocity field in strong turbulence. All standard turbulence statistics presented here are in terms of *spatial* velocity increments $u(x+r,t)-u(x,t)$ at equal times. Time-dependent measurements at a fixed spatial location are interpreted as space-dependent velocities using Taylor's frozen turbulence hypothesis. The validity of this assumption depends on the turbulence levels u'/U and v'/U (where primes indicate rms levels). As discussed later in this paper, the violation of the frozen turbulence hypothesis leads to subtle but significant changes of the spectrum at large wave numbers. If our fractal objects could have infinitely many generations, the stirring of turbulence would be scale

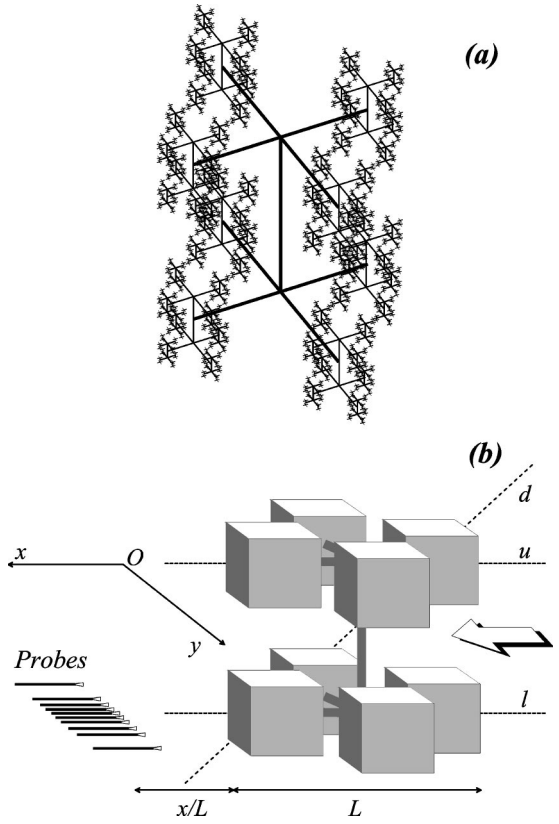

FIG. 1. (a) Schematic representation of the self-similar construction of the fractal objects. (b) Fractal object in a typical measurement configuration. The arrow indicates the direction of the windtunnel flow; the different axes considered are denoted by *u*, *l*, and *d*. In the actual fractal object shown in (a), the cubes are replaced by self-similar copies of the object. For test purposes, an object without this fractal filling was constructed, which can therefore be viewed as a fractal where the self-similar structure was stopped after one iteration.

invariant at scales well within the size of the object. However, due to the flow reversal problem, the probe array cannot be placed closer to the objects than a distance approximately equal to its size L. Consequently, the largest length scale of the object is always in view, and the flow statistics are unavoidably influenced by the largest scale. This circumstance interferes with the geometrical scaling of the object and is responsible for at least part of the experimental observations, as we argue in the following section.

The large-scale imprint on the flow can be altered by rotating the fractal object with respect to the mean velocity. For example, the primary large-scale iterations of the fractal can be shielded by the smaller-scale iterations by rotating the fractal so that its diagonal axis [axis d in Fig. 1(b)] is oriented parallel to the mean flow's x direction. A key point of this work is to separate this large-scale imprint from genuine effects of the object's fractal structure, something which [2] did not do. An overview of the experiments is given in Table I. Most experiments were done on the objects with fractal dimensions $D=2.05$ and $D=2.17$. The object with $D=2.40$, which is more space filling than the other two, has a very turbulent wake, and to avoid flow reversals, measurements could only be done at relatively large distances from the object, $x/L \geqslant 3$. In Sec. V, we report the results of experiments on a test object. In order to compare fractal and nonfractal stirring, the test object [see Fig. 1(b)] has the same large-scale structure as the $D=2.17$ object, but the structure on smaller scales is not filled in: it is a truncated fractal.

TABLE I. The measurements are grouped depending on the fractal dimension D of the object. For each object, different positions in the turbulent wake are probed, with the letters referring to Fig. 1. The object with dimension 3 is a test object that has the same large-scale structure as the $D=2.17$ object, but which is truncated after one iteration.

D	x/L	Configuration	Re_λ	u'/U
2.05	1	*l*	230	0.21
	1.5	*d*	210	0.13
	2	*l*	345	0.20
	2	*u*	370	0.23
	2.8	*l*	310	0.16
2.17	1	*l*	175	0.61
	2	*l*	220	0.34
	2	*l*	215	0.33
	3	*l*	250	0.20
2.40	3	*l*	250	0.43
	5	*l*	650	0.18
3	1	*l*	300	0.25
	1.8	*l*	310	0.16
	2.6	*l*	315	0.12

In order to study the imprint of the large-scale structure of a single object on the wake, we have done experiments with the $D=2.05$ object at various orientations with respect to the mean flow and the probe array at two positions relative to the object's geometric center. In the diagonal orientation [axis d in Fig. 1(b) aligned with the mean flow in the x direction], the projection of the fractal object on a plane perpendicular to the mean flow is more homogeneous. With the velocity probes in the upper position, the support of the fractal is in view (not shown in the figure), therefore, most of the experiments were done behind the lower lobes of the fractal [position l in Fig. 1(b)]. The array of velocity sensors was oriented perpendicular to the mean flow direction and the 10 independent hot-wire sensors were placed such that their 45 distances were distributed approximately exponentially. Consequently, the probes crowd in the center part of the array.

Each of the wires used has a sensitive length of 200 μm and was operated by a computerized constant temperature anemometer. The velocity signals were low-pass filtered at 10 kHz and sampled synchronously at 20 kHz. Each run was preceded by a calibration procedure, in which the voltage to air velocity conversion for each wire was measured using a calibrated nozzle. The resulting 10 calibration tables were updated regularly during the run to allow for a (small) temperature increase of the air in our recirculating windtunnel. Adequate statistical convergence was ensured by collecting velocity readings over 6×10^6 integral time scales in runs that lasted for ≈ 2 h. Repeated runs gave precise reproduction of measured statistics.

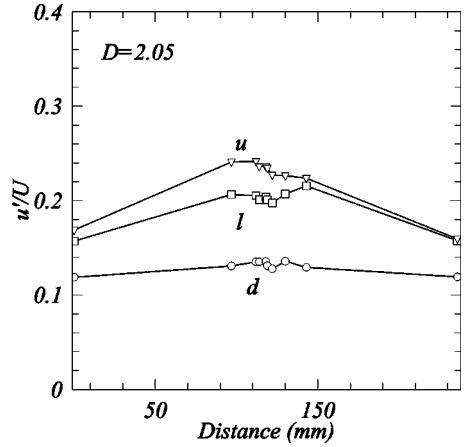

FIG. 2. Turbulence intensity profiles for different configurations of the $D=2.05$ object, recorded at fixed separation $x/L=2$.

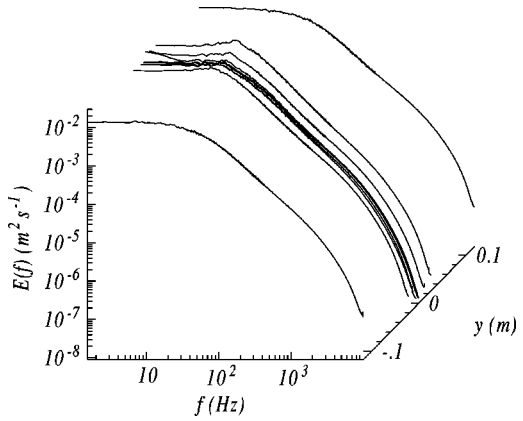

FIG. 3. Turbulence spectra behind fractal object $D=2.05$ at $x/L=2$ and configuration *l*. The low wave number bump in the spectra is more prominent in the central part of the wake.

III. DEPENDENCE ON ORIENTATION

Our purpose is to unravel the finite-size effect of the fractal stirrer on its turbulent wake from the effect of its scale-invariant structure. As the finite-size effect of the stirrer can be expected to depend on its orientation and position with respect to the velocity sensor, we systematically studied the turbulent wake of one fractal object ($D=2.05$) at a fixed separation from that object ($x/L=2$), but at different orientations and with the velocity probes at different vertical positions relative to the object (l and u). These configurations are schematically indicated in Fig. 1(b), with the object: diagonal (d), horizontal with the velocity probes behind the upper lobe (u), and horizontal with the velocity probes behind the lower lobe (l). The properties of the turbulent wakes in each of these three configurations are indicated in Table I, and the turbulent intensity profiles are drawn in Fig. 2. The diagonal orientation not only has the most homogeneous wake and the lowest turbulence levels but also has the smallest turbulence Reynolds number. We conclude that the profiles of the turbulence intensity vary considerably with the orientation of the object.

An overview of the spectra of the u velocity across the wake is given in Fig. 3. There is a clear $k^{-5/3}$ scaling range with a bump at low frequencies reflecting the coherent shedding of vortices. A remarkable observation is that the shedding is very weakly pronounced. In the remainder of this paper, we only show longitudinal spectra and structure functions from the center wire, where the velocity profile is most homogeneous. Throughout, we normalize all turbulence quantities on dissipation scales, $k^*=k\eta/2\pi$, $E^*=E(f)(2\pi/U)\langle\epsilon\rangle^{-2/3}\eta^{-5/3}$, where η is the Kolmogorov length scale, $\langle\epsilon\rangle$ is the mean dissipation rate, and f is the frequency.

The different small k behaviors are more obvious when the spectra are compensated by $k^{5/3}$ and plotted in linear-logarithmic axes, as in Fig. 4. The large-scale region of the spectrum for the object oriented horizontally contains more energy than that for the object oriented diagonally, while all spectra have a well-defined scaling region. Spectra show the large-scale contamination of the wakes by the large scales of the object as low-frequency bumps. This large-scale contamination is virtually absent when the object is diagonally orientated, but Re_λ is too small in that orientation to yield a clear scaling range in structure functions, as shown later in this section. For large wave numbers $k^*\gtrsim 0.1$, the spectra of this object become independent of orientation and position and collapse. Therefore, this part of the spectrum might reflect the intrinsic self-similar structure of the object and may be used to discriminate stirrers with different fractal dimensions. This avenue is explored, in detail, in Sec. IV.

The second-order longitudinal structure function $G_2^L(r)$ is the Fourier companion of the longitudinal spectrum. Still, it is useful to present it because we also have access to the transverse second-order structure function $G_2^T(r)$. Combining $G_2^L(r)$ and $G_2^T(r)$ gives access to the anisotropy of the wake. The exponents of the longitudinal structure functions appear to be close to values normally encountered for approximately homogeneous and isotropic turbulence. We obtain $\zeta_2^L=0.73$, 0.78, and 0.76 for the *d*, *l*, and *u* configurations, respectively.

In the customary longitudinal measurement configuration used so far, velocity increments $\Delta u(\mathbf{r})$ are measured over a

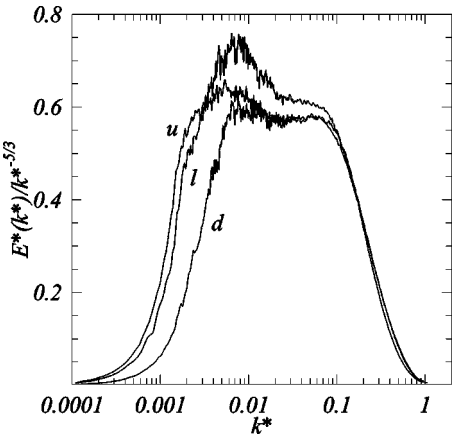

FIG. 4. The compensated longitudinal spectra for different orientations of the $D=2.05$ object and separation $x/L=2$. The low wave number peak is more pronounced for configurations *u* and *l*.

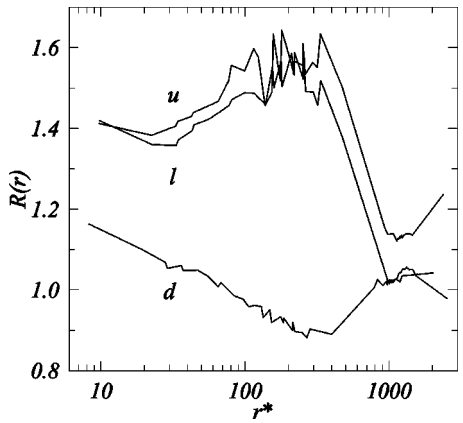

FIG. 5. Anisotropy ratios for different orientations of $D=2.05$ object, measured at separations close to $x/L=2$ behind the object.

separation **r**, where **r** points in the same direction as the measured velocity component *u*. Separations *r* then follow from time delays τ by invoking Taylor's frozen turbulence hypothesis $r=U\tau$. When the turbulence inhomogeneity across the wake is not too large, it is possible to measure the transverse structure functions with the true separation vector **r** oriented perpendicularly to *U*. The transverse second-order structure function scaling exponent is higher for the more inhomogeneous *u* configuration ($\zeta_2^T \sim 0.80$), while for orientation *d* there is no clear indication of a scaling range because the Reynolds number is too small in that case.

In isotropic turbulence, the transverse and longitudinal structure functions are related through

$$\tilde{G}_2^T = G_2^L + \frac{r}{2}\frac{\mathrm{d}G_2^L}{\mathrm{d}r}. \tag{1}$$

The ratio $R(r)=G_2^T/\tilde{G}_2^T$ between the directly measured G_2^T and that computed using Eq. (1) is a measure of the anisotropy. Figure 5 shows the anisotropy of the wake for the three configurations used. As we use the *u* component in both longitudinal and transverse structure functions, $R(r)$ is trivially 1 for large *r* in homogeneous turbulence. The relatively large fluctuations of $R(r)$ in the *u* configuration are not due to lack of statistics, but are a consequence of the flow inhomogeneity across the wake. The horizontal axis of Fig. 5 corresponds to separations $y_i - y_j$ between probes, where y_i and y_j are the locations of the probes. Separations $y_i - y_j$ may be close to separations $y_k - y_l$, but the probes may be in very different regions of the wake. In the diagonal configuration, the wake is more homogeneous and the fluctuations in $R(r)$ are smaller.

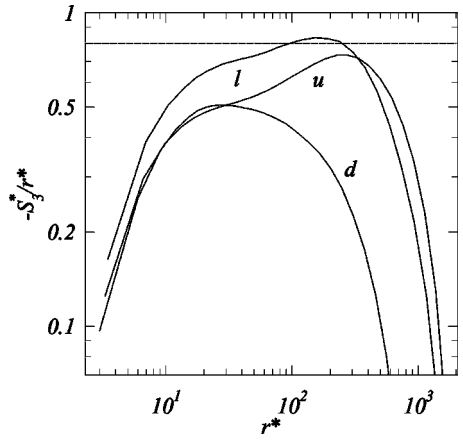

FIG. 6. Third-order structure functions for different orientations of the $D=2.05$ object at separation $x/L=2$. Nonhomogeneous configurations *l* and *d* yield apparent scaling exponents larger than one. The horizontal line compares these results with the $S_3(r) = -4/5\langle\epsilon\rangle r$ Kolmogorov prediction.

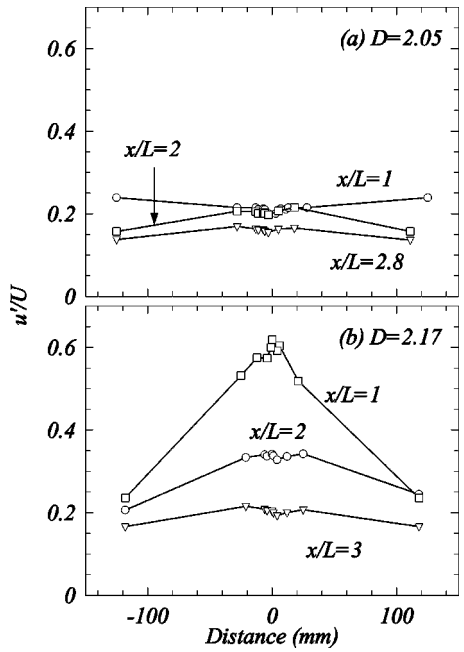

FIG. 7. Turbulence intensity profiles for the (a) $D=2.05$ object and (b) $D=2.17$ object at different separations x/L, all for the same configuration *l* [see Fig. 1(b)]. The intensity of the turbulent wakes produced by the $D=2.17$ object grows significantly stronger as we move closer to the object.

The third-order longitudinal structure functions shown in Fig. 6 have scaling exponents around 1; the nonhomogeneous configurations give ζ_3^L larger than 1, ~ 1.13 and 1.2 for the *u* and *l* positions, respectively, while *d* has $\zeta_3^L \sim 0.9$. Obviously, the small Reynolds number of the *d* configuration results in poor scaling of G_3^L. In the two horizontal configurations, one interpretation of the results might be that the large-scale energy transfer is enhanced, thus leading to an apparent scaling exponent that is significantly larger than unity.

IV. COMPARISON OF $D=2.05$ AND $D=2.17$ FRACTAL OBJECTS

After having exposed the influence of the large-scale structure of the objects on their wake, let us now systematically compare the (apparent) inertial range scaling behavior of the turbulent wakes of two objects, one with fractal dimension $D=2.05$ and the other with $D=2.17$.

We do this by presenting spectra, turbulent intensities and

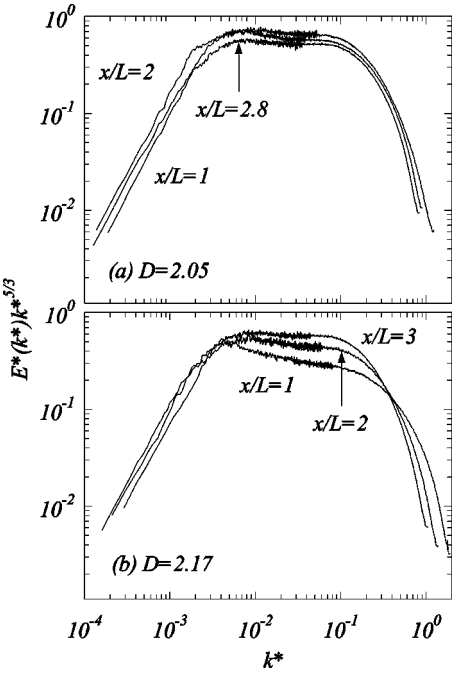

FIG. 8. Comparison between compensated longitudinal spectra for two fractal objects (a) for the $D=2.05$ object and (b) for the 2.17 object. The measurements are done in the lower *l* configuration at different separations behind the object.

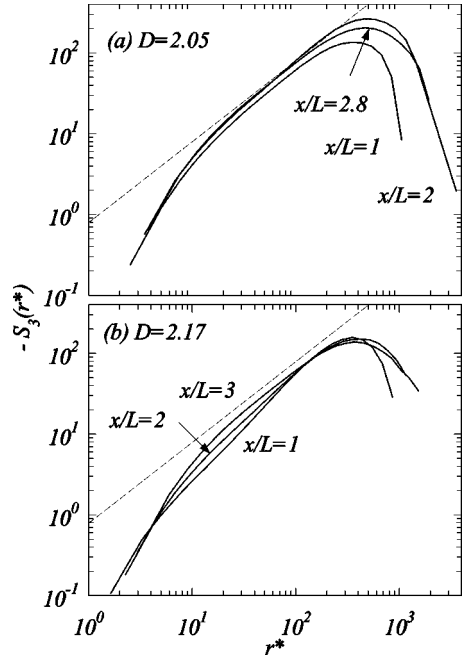

FIG. 9. Third-order structure functions measured for two fractal objects in configuration *l* at different separations x/L (a) for the $D=2.05$ object and (b) for the $D=2.17$ fractal object.

third-order structure functions for increasing separations x/L behind each object at a single orientation *l*, which was chosen because its Reynolds number was typically a factor of 2 larger than for the more homogeneous diagonal configuration *d*, and because it was least influenced by the support of the fractal object. For the object with fractal dimension $D=2.05$, these distances are $x/L=1$, 2 and 2.8, while for the $D=2.17$ case we have $x/L=1$, 2, and 3. The $D=2.17$ object is smaller ($L=26$ cm) than that with $D=2.05$ ($L=37$ cm). The turbulence intensity in the wakes of these two objects is shown in Fig. 7. Although the difference in fractal dimension of the two objects is small, Fig. 7 demonstrates that their wakes are very different. Close to the object at $x/L=1$, the wake of the $D=2.17$ object is much more strongly turbulent and more inhomogeneous than that of the $D=2.05$ object. A remarkable difference is also the way in which the turbulence intensity decreases with increasing distance: the turbulence intensity behind the D=2.17 object decreases much faster with increasing distance, seen in Fig. 7.

The evolution of the energy spectra with increasing distance from the objects is shown in Fig. 8. The energy spectrum corresponding to the $D=2.17$ object has a strong x/L dependence in the range $1\leqslant x/L\leqslant 3$, which is absent in the wake of the $D=2.05$ object.

Not only does the $D=2.17$ object create stronger turbulence (Fig. 7), but it also distributes the turbulent energy over the scales in a different manner. Whilst at small x/L separations, the spectrum of the $D=2.05$ object has a clear $k^{-5/3}$ scaling, that of the $D=2.17$ object has an apparent $E(k)\sim k^{-\alpha}$, with $\alpha>5/3$. Alternatively, the enhancement of $E(k)$ at small k of the $D=2.17$ spectrum may be due to the influence of large-scale shedding. We have checked that, in spite of the high turbulence intensities, minimal flow reversals occur at separation $x/L=1$, while at $x/L=2$ behind the $D=2.17$ object they are absent (flow reversals are also not occurring at all other positions behind both objects where measurements are reported and the turbulence intensity is of the order of 20%).

Despite the relatively small size of the objects and the relatively small Reynolds numbers of their wakes, the third-order longitudinal structure functions in Fig. 9 show clear scaling behavior. For the $D=2.17$ object, the longitudinal $G_3^L(r)$ shows a marked dependence on the distance x/L of the probe array to the fractal object. The scaling behavior of the wake behind the $D=2.17$ object apparently changes with distance x/L. Such a change is virtually absent for the $D=2.05$ object and may be interpreted as a direct influence of the scaling properties of the object on the scaling properties of its wake. A caveat, however, is the small spectral gap which may give rise to a contamination of inertial range behavior by large scales, that is, the large-scale structure of the object. This contamination may be present in the spectra in Fig. 8 and may also affect G_3^L. This is suggestively illustrated in Fig. 10, where we plot side by side $G_3^L(r^*)$ and the energy spectrum as a function of $1/k^*$. It is seen that G_3^L shows similar structure at the same values $1/k^*$ as the spectrum. We conclude that the change of scaling behavior with the fractal dimension of the object should be interpreted with great caution.

In Sec. III, we have seen that the dissipation range of the spectrum is independent of the object's orientation and thus independent of the large-scale structure of the object. In Fig. 11, we plot the spectra of the wakes for the $D=2.05$ and $D=2.17$ objects for various distances x/L. The plot is done such as to emphasize the approximate exponential behavior

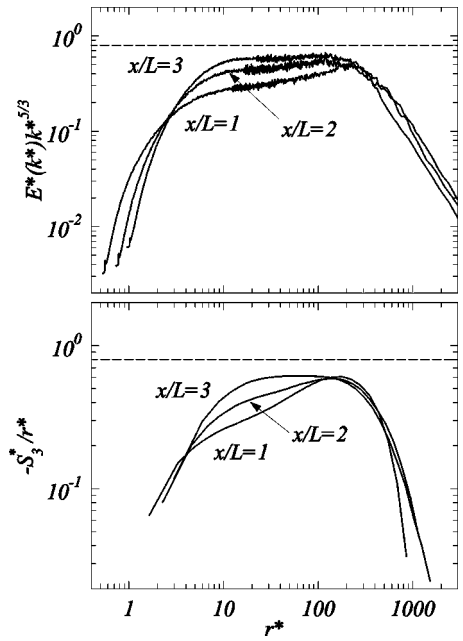

FIG. 10. Third-order compensated structure functions and longitudinal compensated spectra for the $D=2.17$ object. The horizontal axis of the spectra is shown as a function of $1/k^*$.

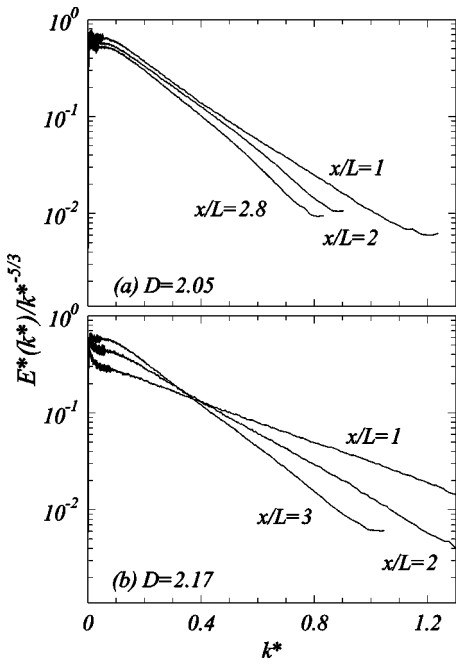

FIG. 11. Dissipative tails of the energy spectra for (a) $D=2.05$ object and (b) $D=2.17$ object measured for configuration *l* and different separations x/L. The logarithmic-linear plot emphasizes the approximate exponential behavior of turbulence spectra tails $E^*(k^*)\sim\exp(-\beta k^*)$.

of the spectrum for dissipative scales $E^*(k^*)\sim\exp(-\beta k^*)$. This well-known exponential behavior can be explained by assuming a linear relation between the energy and its dissipation [3]. In various experiments [4], the exponent β was found to be $\beta\simeq 5.3$.

Figure 11 shows a striking difference between the two objects. Whereas the exponent β remains close to 5.3 for all separations for the $D=2.05$ object, it depends strongly on x/L for the $D=2.17$ case. Perhaps, this is a direct effect of the object's fractal dimension, but now on dissipative scales.

An important caveat is that, with x/L, the turbulence intensity changes, too. As is evident from Table I, this change is much stronger for the $D=2.17$ object than for the $D=2.05$ object, where u'/U is approximately independent of x/L.

We interpret measured spectra as wave number spectra through invocation of the Taylor's hypothesis. As stated in Sec. I, this assumption is challenged more strongly when the turbulence intensity increases. A first correction to the measured spectra arises from the fluctuating part u'/U of the velocity in translating time into space $x=(U+u')\tau$. Due to fluctuations of the advection velocity, the velocity is no longer sampled equidistantly in space and high wave number corrections result. Assuming isotropic spectra, these corrections were worked out in Ref. [5] to first order in u'^2/U^2, for a measured spectrum with an exponential tail $e^{-\beta k^*}$,

$$E^{real}(k^*)=\left[1-\frac{1}{2}\left(\frac{u'}{U}\right)^2\left(\frac{22}{9}+\frac{10}{3}\beta k^*+(\beta k^*)^2\right)\right]E^{meas}(k^*), \qquad (2)$$

where E^{real} is the underlying true spatial spectrum and E^{meas} is the measured spectrum through the use of Taylor's hypothesis.[1] Assuming an underlying spectrum $E^{real}(k^*)$ with a shape that does not change with the turbulent intensity u'/U, Eq. (2) predicts that the shape of the measured spectrum $E^{meas}(k^*)$ depends on the turbulence intensity. Actually, this dependence is such that the measured β *decreases* with increasing intensity, just as is observed in Fig. 11. In Fig. 12, we assume a real spectrum with $E(k^*)\sim e^{-5.3k^*}$, compute its appearance in the turbulence levels encountered in our experiment and compare it to the actually measured spectra. It appears that Eq. (2) can explain the measured dependence of β on u'/U albeit qualitatively rather than quantitatively. It must be noted, however, that the turbulence level in our experiment can be as high as 60%, whereas Eq. (2) is only first-order in $(u'/U)^2$.

These observations make it difficult to establish a direct relation between the dissipative properties of the wake and the fractal dimension of the object, other than a trivial effect of the increased turbulence intensity.

V. TURBULENT WAKE OF A TRUNCATED FRACTAL

In the preceding section we compared the turbulent wakes of two fractal objects that had different fractal dimensions. We found significant differences between the wakes shed off these different fractal dimensions. A much cruder test is to

[1]This relation holds for the one-dimensional projection of the spectrum.

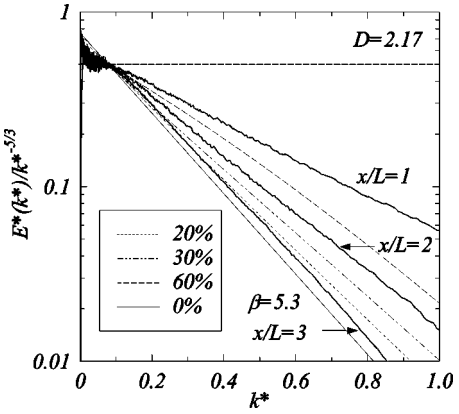

FIG. 12. Comparison between the measured spectra tails for the $D=2.17$ object and effects of correction to the Taylor hypothesis. Full lines, measured spectra at $x/L=1$ (turbulence intensity $u'/U=61\%$), $x/L=2$ ($u'/U=34\%$), and $x/L=3$ ($u'/U=20\%$). Dashed lines, spectra computed from Eq. (2) by assuming an underlying spectrum $E^*(k^*)\sim\exp(-\beta k^*)$ with $\beta=5.3$ at various turbulence intensities.

compare these wakes to the wake shed by a nonfractal object. To this aim, we constructed an object that has the same large-scale structure as the $D=2.17$ object, but that lacks its fractal structure, i.e., we stopped at the first iteration of the self-similar refinement. The large-scale dimensions of this object are the same as those of the $D=2.17$ fractal.

We studied the turbulent wake of this object through turbulence measurements similar to those performed on fractals. Accordingly, its scaling properties were investigated in the configuration *l*, at varying separations behind the object $x/L=1$, 1.8, and 2.6.

The characteristics of the turbulent wakes are listed in Table I; while the Reynolds numbers are comparable to those of the fractal objects, the turbulence intensities are smaller. This clearly demonstrates that it is not their large-scale structure that makes fractal objects better turbulence generators, but their (self-similar) refinement of length scales.

The inertial range scaling properties of the wake of the truncated fractal object are very different from those of the true fractal object. The third-order structure functions, shown in Fig. 13, no longer depend on the x/L separation and now

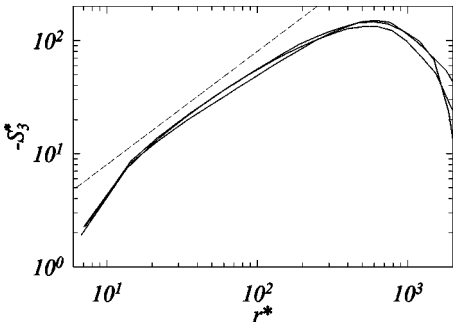

FIG. 13. Third-order longitudinal structure functions measured in the wake of a truncated fractal at separations $x/L=1$, 1.6, and 2.6 in configuration *l*. The dashed line is the $-(4/5)r^*$ exact result for isotropic and homogeneous turbulence.

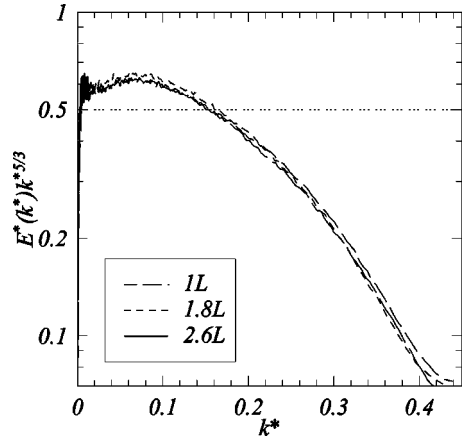

FIG. 14. Large wave number tails for the turbulent wake of a truncated fractal, measured in configuration *l* at three increasing separations $x/L=1$,1.6, and 2.6, as indicated in the legend.

have an apparent slope *less* than 1, compared to the structure functions in Fig. 9(b). In Fig. 14, we compare the large wave number behavior of the longitudinal spectra for three positions x/L in the wake of the truncated fractal object. These positions are comparable to those used for the self-similar fractal objects in Fig. 11. As for the third-order structure functions, also the dissipative tails of the spectra now become independent of the separation x/L. This can only partly be explained by the reduced turbulence intensities of the truncated fractal wake, which range from $u'/U=0.25$, at the smallest separation $x/L=1$, to $u'/U=0.12$ at $x/L=2.6$.

VI. CONCLUSIONS

We can clearly distinguish between the scaling properties of turbulence stirred by a fractal object that has a range of refined scales and that of a truncated fractal. However, for self-similar fractals, we found it difficult to conclude a relation between the dimension of the object (which quantifies the manner of refinement) and the scaling properties of the turbulent wake.

We have observed suggestive effects in the measured spectra and structure functions, but they could not be firmly distinguished from the influence of the finite size of the objects. In order to achieve such clear distinction, we need larger Reynolds numbers and/or larger fractal objects that fill the windtunnel cross section. In this respect, it is interesting to point to recent work where a plane grid with a few scales (but not a fractal) was found to produce high Reynolds numbers (Ref. [6]).

While we may not have yet achieved our goal, we have found a few remarkable large-scale properties of wakes shed by fractal objects. Vortex shedding off fractal objects has a very weakly pronounced energy spectrum signature. It is even possible to rotate the fractal objects so as to nearly fully inhibit this vortex shedding signature but at the cost of very significantly lowering the Reynolds number of the turbulence

in the wake. In our experiment, such an orientation had the effect of somehow shielding the largest-scale features of the fractals and resulted in a Reynolds number too low for a well-defined scaling range to be seen in the third-order longitudinal structure function. It is puzzling, however, that the energy spectrum of the lowest fractal dimension object ($D=2.05$) in that orientation does exhibit a decade of fairly well-defined $k^{-5/3}$ scaling.

ACKNOWLEDGMENTS

We gratefully acknowledge financial support by the ''Nederlandse Organisatie voor Wetenschappelijk Onderzoek (NWO)'' and ''Stichting Fundamenteel Onderzoek der Materie (FOM).'' We are indebted to Gerard Trines, Ad Holten, and Gerald Oerlemans for technical assistance. J.C.V. acknowledges the support of the Royal Society.

[1] F. Okkels, B. Mazzi, and J. Vassilicos, Eur. Phys. J. B **28**, 243 (2002).

[2] D. Queiros-Conde and J. Vassilicos, in *Intermittency in Turbulent Flows*, edited by J. Vassilicos (Cambridge University Press, Cambridge, 2001), pp. 136–167.

[3] S. Pope, *Turbulent Flows* (Cambridge University Press, Cambridge, 2000).

[4] S.G. Saddoughi and S.V. Veeravali, J. Fluid Mech. **268**, 333 (1994).

[5] E. Gledzer, Physica D **104**, 163 (1997).

[6] B. Pearson, P.-A. Krogståd, and W. van de Water, Phys. Fluids **14**, 1288 (2002).